# A new catalysts for the MeOH to DME reaction: Reaction mechanism and kinetic behavior

Cavus Falamaki, Morteza Sohrabi , Sayed Javid Royaee and Sayed Siamak Ashraf Talesh
Chemical Engineering Department, Amirkabir University of Technology, Hafez Ave. , P.O. Box 15875-4413, Tehran, Iran

## Abstract

The kinetic behavior of a modified clinoptilolite zeolite for the methanol to dimethylether dehydration reaction has been investigated using a differential fixed bed reactor. It was observed that at high partial pressures, MeOH plays an inhibition role. A novel Langmuir-Hinshelwood type reaction mechanism has been developed that predicts the latter effect .The modified clinoptilolite zeolite subject of this study might be of high industrial interest because of the relative lower activation energy (ca. 60 kJ $mol^{-1}$ ) compared to other reported zeolitic and non-zeolitic catalysts.

## Introduction

Natural zeolites like clinoptilolites are 'inherent' potential candidates for the production of catalysts. The reasons are multiple: 1) If protonated, they may exhibit a 'natural' hybrid character due to the presence of embedded metal oxy-hydroxides [1-2], especially Mg compounds 2) Enormous deposits of relatively pure and easy to mine tuffs exist all over the world 3) As a result of a natural genesis process, clinoptilolite micrometer sized crystals are held together by a natural binder, in most of the cases silica polymorphs, thus eliminating the need for an agglomeration-granulation process for the production of the final catalyst product. These matrixes posses adequate macro-porosity allowing reacting species reach the channels easily 4) From a catalytic engineering point of view, clinoptilolites belong to the medium pore size zeolites [0.45-0.60 nm] making them proper candidates for catalyzing important petrochemical reactions like methanol dehydration.

Armbruster [5] extrapolated in 2001 that in the coming years 'natural' zeolites would become less important for catalytic applications. The authors of this work are not of the same opinion and this is rationalized according to the following discussion. Falamaki et al [6] have recently patented a successful modification procedure for converting natural Iranian clinoptilolite to an efficient catalyst for the dehydration reaction of methanol to dimethylether (MTD). This modification was optimized according to a Taguchi experimental design method which has been reported in a separate paper by Royaee et al [7].

One of the most important aspects of their discovery was a selectivity over 99.7 % obtained at industrial operational conditions (16 bar pressure). It is the opinion of the authors of this work that excluding a

* **Corresponding author.**

catalyst production plant and, instead, easily modifying a natural product at
large scale might be an environmental-friendly approach to the catalyst manufacture technology. On the other hand, developing countries like Iran are getting more and more aware of their natural resources and try to exploit them.

The MTD process is of great industrial interest. Dimethylether may be produced by two general processes: Catalytic dehydration of methanol (MTD) and direct conversion of natural gas.

The former process has been fully industrialized since the last decade and the latter process is still under development for shifting from pilot to full industrial scale. Development of new and more economic catalysts for the MTD process is of great industrial interest. In addition, the MTD process is part of the methanol to olefin (MTO) and methanol to gasoline (MTG) processes. This is why the theory of methanol activation and kinetic behavior, especially for zeolitic materials (mostly H-ZSM5), has been subject of extensive studies in the past [8-13].

The present work investigates the kinetics of the catalytic methanol dehydration process over a modified natural clinoptilolite zeolite using a differential fixed bed catalytic reactor. It should be mentioned that no such kinetic analysis has ever been published in open literature. The kinetic behavior of the catalyst in the absence of bulk gas film resistance and macro-pore resistance in the temperature range of 310-350 ˚C has been thoroughly investigated. A novel reaction mechanism has been proposed that predicts the abnormal methanol inhibition effect at high partial pressures along the inhibition effect of water. The activation energy of the reaction has been calculated.

**Experimental**

The characteristics' of the clinoptilolite zeolite raw material used throughout this study have been recently reported elsewhere [7]. Briefly, it is has an HEU structure type with a Si/Al ratio of 5.78 and the inorganic binder (less than 10 wt. %) consists mainly of quartz and cristobalite. The raw material was transformed into catalyst according to the following procedure:

The raw zeolite was crushed and mesh separated into 6 classes of average size of 80, 100, 125, 225, 525 and 800 μm. Afterwards the powders were subjected to ion-exchange with 2 N ammonium chloride (MERCK) solution (15 g zeolite per 1 liter salt solution) for 24 h under vigorous agitation at room temperature. The resultant powders were filtered washed with hot distilled water and the whole process was repeated again. The final powders were dried overnight at 100 ˚C and further calcined at 500 ˚C for 3 h.

Catalytic experiments were performed using the catatest scheme presented in figure 1. The plug flow reactor had an internal diameter of 15 mm and a height of 70 cm. About 45 cm of the upper part of the reactor was filled with ceramic packing (silicon carbide). The latter acted as evaporator and gas pre-heater. The reactor was filled with 1 g catalyst between two stainless steel meshes (70 μm pore size) resulting in an approximate catalyst bed depth of 5 mm. The bottom part of the reactor height was similarly filled with ceramic packing. Initial activation of the catalyst prior to kinetic investigation was performed by purging $N_2$ at 400 ˚C for 45 min at a flow-rate of 100 $cm^3$ $min^{-1}$. Afterwards the temperature of the reaction zone was reduced to that of the desired reaction temperature (310, 330 and 350 ˚C) and the predetermined methanol and $N_2$ flow rates were implemented. In some of the experiments, 'initial' water was introduced by dissolving distilled water in proper amount in the vessel containing methanol. Experiments were run under atmospheric pressure. Methanol concentration was varied in the range of 20-85 mol %. Experiments performed with 'initial" water had a water concentration of 13 mol %.The effluent gas from the phase separator was analyzed on-line with a GC (6890N, Agilent) using an HP-Plot Q capillary column (30 m) at 10 min intervals. Based on GC analysis, the steady-state reaction condition was established between 2.5 to 6 h, depending on the flow-rates imposed.

FTIR analysis of raw and modified catalyst samples was performed using a SUPER AQUARIUS apparatus. Assessment of zeolite acidity was performed using $NH_3$ temperature

programmed desorption (TPD). For this means 0.2 g of the catalyst was subjected to the following treatments: a) Purging He gas with a flow rate of 30 $cm^3$ $min^{-1}$ with simultaneous heating with a ramp rate of 10 ˚C $min^{-1}$ up to 430 ˚C with a dwelling time of 180 min b) adsorption of $NH_3$ using a purge gas flow rate of 40 $cm^3$ $min^{-1}$ isothermally at 100 ˚C with subsequent dwelling time of 90 min c) desorption of $NH_3$ using He carrier gas at a flow rate of 40 $cm^3$ $min^{-1}$ employing a ramp rate of 10 ˚C $min^{-1}$ up to 650 ˚C followed by a dwelling period of 20 min. A TPD/TPT Micromeritics apparatus with a thermal conductivity detector was used.

**Results and discussion**

- Catalyst characterization

FTIR spectra of the raw zeolite and the produced catalyst are shown in figure 2 (a-b). It is observed that the raw natural zeolite shows an adsorption band in the region near 3623 $cm^{-1}$. The bands in the 3600-3650 $cm^{-1}$ region are usually attributed to bridging hydroxyls (free bridging hydroxyls or Brønsted acid sites) [14]. Therefore, the raw material might have 'intrinsic' catalytic activity. Sakoh et al. [15] reported a conversion level of 91.4 % of MeOH at a temperature of 350 ˚C for a natural zeolite in its original form. Isomeration of α-pinene over calcined natural zeolites is another testimony for the natural solid-acidity of these materials [16]. An important fact is the attenuation of the band region cited above upon ion-exchange with ammonium chloride and subsequent calcination (figure 2-b). This phenomenon may be attributed to the transformation of the Brønsted to Lewis acid sites as a result of dehydration reactions at 773 K. The disappearance of bands with a wave number larger than 3625 $cm^{-1}$ is attributed to condensation reactions occurred between different kinds of hydroxyl groups during calcination at 500 ˚C. Calcination has been reported to attenuate intensities in the region of 3400-3700 $cm^{-1}$ for natural clinoptilolite at 600 ˚C [16].

The TPD diagram of the catalyst is shown in figure 3. The resulting curve has a distinct maximum below 200 ˚C with a decaying tail up to near 600 ˚C. The total desorption volume is 0.489 $cm^3$ which corresponds to 0.1 mmol $NH_3$ (g catalyst)$^{-1}$). This trend might be attributed to the prevalence of weak acid sites (Lewis sites) over the stronger acidic sites (Brønsted). This is desired for the MTD reaction as it is generally accepted that Lewis acidic sites are responsible for the main reaction and that Brønsted acidic sites induce deleterious side reactions. The latter reactions might promote catalyst deactivation and reduce selectivity.

It should be mentioned that GC analysis showed that no side product (hydrocarbons) was produced in any of the experiments whose details will be presented in the following sections. We attribute this to the dominance of Lewis acid sites, as stated above.

- Assessment of bulk gas phase film resistance

Despite having applied micrometer size catalyst particles, it was indispensable to establish the proper process parameters for ensuring the absence of film resistance effects in the bulk gas phase prior going through any detailed kinetic investigation. For this means a series of experiments were run using 100 μm particles at a reaction temperature of 330 ˚C which details are summarized in table I. For the methanol concentrations of 20, 35, 50, 70 and 80 mole %, average reaction rates for two total feed gas flow rates (the absolute amount of flow rate change being 33.33 % in each case) has been reported. Based on the experimental results shown in table I, it is observed that the absolute change in average reaction rate is less than 6 % for all the cases.

Accordingly, it may be confidently stated that film resistance in the bulk gas phase does not control the total reaction rate for the 100 μm catalyst particles.

- Assessment of macro-pore gas phase film resistance

At a second stage, it was necessary to assess film resistance in the particles macro-pores. Actually the particles consist of a porous matrix embedding zeolite crystals smaller than 10 μm and connecting them through macro-pores. The controlling reaction rate should be independent of the length of the macro-pores, and as a corollary, of the size of the particles. Macro-pore film resistance was evaluated by running a series of experiments for different catalyst particle sizes and the constant process parameters as follows: Reaction temperature 330 ˚C , methanol flow rate of 0.9 $cm^3\ min^{-1}$ and nitrogen flow rate of 538 $cm^3\ min^{-1}$ (corresponding to a methanol partial pressure of 0.5 atm). Table II summarizes the corresponding results. By extrapolating the reaction rate for a particle size of zero μm size using a polynomial of order 6, a limiting reaction rate value was calculated. Based on this value, the effectiveness factor η has been evaluated as a function of particle size and is shown in figure 4. It is observed that for particle sizes equal or smaller than 100 μm the effectiveness factor is larger than 0.99 and the macro-pore film resistance may be safely neglected. Accordingly, a particle size of 100 μm was selected for the kinetic investigation study. Using smaller particles was accompanied with a higher risk of particle egress from the system as dust.

- Kinetic investigation (without initial water partial pressure)

The process parameters used for the kinetic investigations in the case of no initial water partial pressure are reported in table III. The conversions achieved are also reported in the latter table and, as it can be observed, all the average conversions measured are less than 0.024. The latter observation confirms the 'differential' state of the reactor which consequently allows us to consider isothermal state throughout the reactor (despite the reaction being highly exothermic). In addition, the use of the following simple relation for the calculation of the reaction rate from conversion values is justified:

$$(-r_A)_{avg} = \frac{F_{A0}\ (X_{A,out} - X_{A,in})}{W} \qquad (1)$$

where $(-r_A)_{avg}$ is the average reaction rate throughout the reactor (mole $g^{-1}\ min^{-1}$), $F_{A0}$ the initial total feed rate (mole $min^{-1}$), $X_{A,out}$ the conversion in the outlet stream, $X_{A,in}$ the conversion in the feed, and W is the weight of the catalyst (g). The conversion value reported in table III is simply the average value between $X_{A,out}$ and $X_{A,in}$.

Figure 5 show the calculated reaction rates as a function of reaction temperature and MeOH average partial pressure. A general trend is observed for each of the reaction temperatures applied. For the experiments performed at 310 and 330 ˚C, the reaction rate increases with MeOH partial pressure increase during the interval of 0.2-0.5 atm for the average pressure of MeOH. For partial pressures higher than 0.6 atm, the trend is opposite. The partial pressure threshold was 0.7 atm for the reactions preformed at 350 ˚C. In the only published report on the kinetics of MeOH dehydration to dimethylether over natural zeolites by Bandiera and Naccache [17], such an abrupt decrease has not been reported. Actually the latter work did not cover the wide range of MeOH partial pressures considered in the present work. Nonetheless, their reported data show a slight decreasing trend of the reaction rate at high partial pressures at the reaction temperatures of 250

and 300 ˚C. Figure 5 clearly shows that there exists some sort of 'inhibiting' effect at high MeOH partial pressures in the reaction temperature range of 310-300 ˚C.

No such significant MeOH "inhibiting" effect at high partial pressures has ever been reported in the literature in the past for methanol dehydration catalysts like gamma-alumina, amorphous silica alumina, zeolites and macro-reticular cation exchange resins [17-22]. On the other hand, both Eley-Rideal and Langmuir-Hinshelwood type reaction mechanisms have been proposed for the catalytic dehydration reaction of methanol [17-22]. None of the proposed reaction mechanisms in open literature could predict the strong MeOH inhibiting trend at high partial pressures of concern. Due to the general shape of the reaction rate versus MeOH partial pressure it was found logical to try propose a Langmuir-Hinshelwood type mechanism which could involve the inhibiting effect of MeOH in a rationale way. Our proposed mechanism is as follows:

$$M_{(g)} + S \Leftrightarrow M.S^{*} \qquad (2)$$

$$M.S^{*} + mM \Leftrightarrow M_{m}(M.S) \qquad (3)$$

$$M.S^{*} + nW \Leftrightarrow W_{n}(M.S) \qquad (4)$$

$$W + S \Leftrightarrow W.S \qquad (5)$$

$$2\,M.S \Leftrightarrow D_{(g)} + W.S + S \qquad (6)$$

where $M_{(g)}$ is MeOH in gas phase, M . $S^{*}$ is an active intermediate involving bonding between the unique zeolite surface species and adsorbed MeOH, $M_m$(M.S) and $W_n$(M.S) are 'inactive' intermediate species (m and n are integer number equal or larger than 1), W is water, $D_{(g)}$ is dimethylether in gas phase and W.S represent adsorbed water on free catalyst acidic sites.. The innovation of the proposed mechanism lies in the fact that we allow some sort of 'deactivation' or neutral behavior of the acidic sites at high MeOH (and also water) partial pressures. The reactive intermediate $M.S^{*}$ may become an inactive one by adsorbing m molecules of MeOH (reaction 3) or n molecules of water (reaction 4) from the gas phase.

The resulting rate equation may be derived as follows:

$$-(r_M) = \frac{k_r K_M^{2} P_M^{2} - k_r' K_W P_D P_W}{(1 + K_M P_M + K_W P_W + K_N K_M P_M^{m+1} + K_{NN} K_M P_M P_W^{n})^{2}} \qquad (7)$$

where $k_r$ and $k'_r$ are the forward and backward reaction rate constants of reaction (6) (mole $min^{-1}$), $K_M$ is the adsorption equilibrium constant of reaction (2) ($atm^{-1}$), $K_W$ is the adsorption equilibrium constant of reaction (5) ($atm^{-1}$), $K_N$ is the adsorption equilibrium constant of reaction (3), $K_{NN}$ is the adsorption equilibrium of reaction (4), $P_M$ is the partial pressure of MeOH (atm), $P_D$ the partial pressure of dimethylether (atm) and $P_W$ is the partial pressure of water (atm).

The expected inhibiting behavior at high MeOH partial pressures comes into force at high $P_M$ values due its extra power of m+1 in the denominator.

Table IV shows the result of parameter optimization for the reaction scheme presented. Figures 6 a-b show the simulated reaction rates as a function of average MeOH partial pressure and reaction temperature for two different sets of values of m and n: a) m = 1, n = 1 and b) m = 3, n = 1. It is observed that in both cases the general trend of the simulated curves obeys the experimental one. Nonetheless, it is clearly observed that the curves corresponding to set b result in a better agreement between experimental data and simulated curves. It is the opinion of the

authors of this work that interaction between $MS^*$ active intermediate species actually can occur for different values of m and n simultaneously, therefore optimum values of m = 3 and n = 1 represent "average" values from two statistical populations.

The values obtained for $k'_r$ are at least three order of magnitude smaller than the corresponding values for $k_r$. Therefore the reverse reaction (6) may be neglected. On the other hand, the obtained values for $K_W$ are at least eight order of magnitude smaller than the corresponding values of $K_M$. This means that the adsorption of water on free catalytic sites is negligible with respect to the adsorption of water molecules on $MS^*$ active intermediate complexes.

According to the previous discussions, equation (7) may be simplified to the following final form:

$$-(r_M) = \frac{k_r K_M^{\ 2} P_M^{\ 2}}{(1 + K_M P_M + K_N K_M P_M^{\ 4} + K_{NN} K_M P_M P_W)^2} \qquad (8)$$

Based on table IV, the activation energy of the forward of equation (6) has been calculated to be 60.83 and 59.68 kJ $mol^{-1}$ for sets a and b, respectively. Bandiera and Naccache [17] have reported a value of 80.3 kJ $mol^{-1}$ for the MTD reaction over H-mordenite in the temperature range of 250-300 ˚C. It should be reminded that reported activation energies for γ-alumina, silica-alumina and ion-exchange resin catalysts have been reported to be larger than 100 kJ $mol^{-1}$ [18]. Thus, due to relatively low activation energy, the clinoptilolite catalyst investigated throughout this work may be considered a proper candidate as a catalyst for the MeOH to DME dehydration process.

`

- Effect of water on kinetic behavior

Figures 7 a-b show the effect of the presence of initial water on the MTD reaction rate for the reaction temperatures 310 and 350 ˚C at various MeOH partial pressures. Compared to the corresponding points in figure 5 the inhibiting effect of water is observed to be significant in all the experiments. The simulated results based on the parameter values presented in table IV result in a reasonable agreement with the experimental data. In the case of 'initial water' the two sets a and b result in approximately similar results. This is in accordance with the fact that the inhibiting effect of MeOH should be less pronounced due to the relative high amount of water present. In other words, simulated results are less sensitive to the value of m. Therefore, we suppose that the novel reaction model presented is highly robust as it can successfully predict both the methanol and water inhibition effects.

## Conclusions

The kinetic behavior of a modified clinoptilolite zeolite for the MTD reaction had been investigated using a differential fixed bed reactor. It was observed that at high partial pressures, MeOH plays an inhibition role. A new Langmuir-Hinshelwood model was presented based on a reaction mechanism that incorporates the latter effect and is also able to predict the inhibitory effect of water if present at high concentrations. The creation of inactive intermediates like $M_m(M.S)$ and $W_n(M.S)$ should be verified using in-situ analysis methods in future to provide a

robust theoretical support for the proposed model. It is noteworthy that, as far as the attenuating effect of MeOH is considered, there exists a strong resemblance between the reaction mechanism proposed and the uncompetitive inhibition reaction mechanism of enzymatic reactions. It should be stressed out that the inhibiting action of MeOH does not mean that the catalyst results in unacceptable yields in real operating conditions and this has been addressed previously in the paper of Royaee et al. [7].

The modified clinoptilolite zeolite subject of this study might be of high industrial interest because of the relative lower activation energy (ca. 60 kJ $mol^{-1}$ ) compared to other zeolitic and non-zeolitic catalysts.

The study of the deactivation behavior of the described catalyst is the subject of our future works before deciding to run fixed bed pilot scale experiments.



**References**


1. D. Mao, M. Yang, J. Xia, B. Zhang, Q. Song and Q. Chen, Highly effective hybrid catalyst for the direct synthesis of dimethylether from syngas with magnesium oxide-modified HZSM5 as a dehydration compound, J. Catal., 230 (2005) 140-149.
2. T. K. Katranas, A. G. Vlessidis, V. A. Tsiatorous, K. S. Triantafyllidis and N. P. Evmiridis, Dehydrogenation of propane over natural clinoptilolite zeolites, Mic. Mes. Mat., 61 (2003) 189-198.
3. M. W. Ackley and R. T. Yang, Diffusion in ion-exchanged clinoptilolites, AIChE Journal, 37 (1991) 1645-1656.
4. M. W. Meier and D. H. Olson, Atlas of zeolite structure types, 3rd edt., Butterworth-Heinemann, 1992, p. 138.
5. T. Armbruster, Clinoptilolite-Heulandite: Applications and basic research, Stud. Surf. Sci. Cat., 135 (2001) 13-17.
6. C. Falamaki, M. Sohrabi, and S. S. Ashraf-Talesh, Manufacture of a catalyst for the methanol to dimethylether conversion process via a natural zeolite from the HEU structure type, Iranian Patent 38098, 2006.
7. S. J. Royaee, M. Sohrabi and C. Falamaki, Methanol dehydration to dimethylether using modified clinoptilolite, Mat. Sci., in press (2007).
8. C. M. Zicovich-Wilson, P. Viruela and A. Corma, Formation of surface methoxy groups on H-zeolites from methanol: A quantum chemical study, J. Phy. Chem., 99 (1995) 13224-13231.
9. S. R. Blaszkowski and R.A. van Santen, Density functional theory calculations of the activation of methanol by a Broensted zeolitic proton, J. Phy. Chem., 99 (1995) 11728-11738.

10. T. Y. Park and G. F. Froment, Kinetic modeling of the methanol to olefin process. 1. Model formulation, Ind. Eng. Chem. Res., 40 (2001) 4172-4186.
11. W.-Z. Lu, L.-H. Teng and W.-D. Xiao, Simulation and experimental study of dimethylether synthesis from syngas in a fluidized-bed reactor, Chem. Eng. Sci., 59 (2004) 5455-5455.
12. D. Mao, W. Yang, j. Xia, B. Xiang, Q. Song and Q. Chen, Highly effective hybrid catalyst for the direct synthesis of dimethylether from syn-gas with magnesium oxide-modifed H-ZSM-5 as a dehydration component, J. Cat., 230 (2005) 155-164.
13. L. K. Carlson, P. K. Isbester and E. J. Munson, Study of the conversion of methanol to dimethylether on zeolite HZSM-5 using in situ flow MASS NMR, Sol. State Nuc. Mag. Res., 16 (2000) 93-102.
14. A. Yentys and J. A. Lercher, Techniques of zeolite characterization, in Introduction to Zeolite Science and Practice, H. van Bekkum, E. M. Flanigen, P. A. Jacobs and J. C. Jansen (editors), Stud. Surf. Sci. Catal., Vol. 137, p. 370.
15. H. Sakoh, M. Nitta and K. Amura, Catalytic activity and selectivity of modified clinoptilolites for conversion of methanol to light olefins, Appl. Catal., 16 (1985) 249-253.
16. O. Akpolat, G. Gunduz, F. Ozkan and N. Besun, Isomeration of α-pinene over calcined natural zeolites, Appl. Catal. A: General, 265 (2004) 11-22.
17. J. Bandiera and C. Naccache, Kinetics of methanol dehydration in dealuminated H-mordenite: Model with acid and base active centers, Appl. Catal., 69 (1001) 139-148.
18. G. Bercic and J. Levec, Intrinsic and global reaction rate of methanol dehydration over γ-alumina pellets, Ind. Eng. Chem. Res., 31 (1992) 1035-1040.
19. G. Bercic and J. Levec, Catalytic dehydration of methanol to dimethylether. Kinetic investigation and reactor simulation, Ind. Eng. Chem. Res., 32 (1993) 2478-2484.
20. G. Schmitz, Deshydration du methanol sur silice-alumine, Chim. Phys., 75 (1978) 650-655.
21. B. C. Gates and L. N. Johanson, Langmuir-Hinshelwood kinetics of the dehydration of methanol catalyzed by cation exchange resin, AIChE J., 17 (1971) 98-100.
22. K. Klusacek and P. Schneider, Stationary catalytic kinetics via surface concentrations from transient data: Methanol dehydration, Chem. Eng. Sci., 37 (1982) 1523-1528.

Table I. Process parameters and results for the experiments performed for evaluating bulk gas phase film resistance.

| MeOH mole % | MeOH flow rate (a) $cm^3min^{-1}$ | $N_2$ flow rate (a) $cm^3min^{-1}$ | MeOH flow rate (b) $cm^3min^{-1}$ | $N_2$ flow rate (b) $cm^3min^{-1}$ | reaction rate (a) mole $g^{-1}$ $min^{-1}$ | reaction rate (b) mole $g^{-1}$ $min^{-1}$ | feed flow rate change % | reaction rate change % |
|---|---|---|---|---|---|---|---|---|
| 20 | 0.3 | 716.76 | 0.2 | 477.84 | 0.000176 | 0.000175 | -33.33 | -0.49 |
| 35 | 0.6 | 665.57 | 0.4 | 443.71 | 0.000213 | 0.000225 | -33.33 | 5.59 |
| 50 | 0.9 | 537.84 | 1.2 | 717.12 | 0.000258 | 0.000249 | 33.33 | -3.79 |
| 70 | 1.2 | 307.18 | 0.8 | 204.79 | 0.000279 | 0.000266 | -33.33 | -4.41 |
| 85 | 1.5 | 158.11 | 1.0 | 105.40 | 0.000214 | 0.000209 | -33.33 | -1.86 |

Table II. Process parameters and results for the experiments performed for evaluating macro-pore gas phase film resistance.

| particle size (μm) | conversion | reaction rate (mole $g^{-1}$ $min^{-1}$) |
|---|---|---|
| 80 | 0.010308 | 0.00023 |
| 125 | 0.010253 | 0.000229 |
| 225 | 0.010095 | 0.000226 |
| 525 | 0.00967 | 0.000216 |
| 800 | 0.008775 | 0.000196 |

Table III. Process parameters and measured conversion for the kinetics tests (no initial water partial pressure)

| MeOH (mole %) | MeOH flow rate ($cm^3min^{-1}$) | nitrogen flow rate ($cm^3min^{-1}$) | reaction temperature (°C) | average conversion |
|---|---|---|---|---|
| 20 | 0.30 | 716.76 | 310 | 0.0144 |
| 35 | 0.60 | 665.57 | 310 | 0.0089 |
| 50 | 0.90 | 537.84 | 310 | 0.0061 |
| 20 | 0.30 | 716.76 | 330 | 0.0181 |
| 35 | 0.60 | 665.57 | 330 | 0.0125 |
| 50 | 0.90 | 537.84 | 330 | 0.0103 |
| 20 | 0.30 | 716.76 | 350 | 0.0238 |
| 35 | 0.60 | 665.57 | 350 | 0.0145 |
| 50 | 0.90 | 537.84 | 350 | 0.0117 |

Table IV. Optimal calculated parameters for relation 7.

| temperature (°C) | $k_r$ mole $min^{-1}$ x $10^4$ | $k_r'$ mole $min^{-1}$ x $10^8$ | $K_M$ $atm^{-1}$ | $K_W$ $atm^{-1}$ x $10^7$ | $K_N$ $atm^{-1}$ | $K_{NN}$ $atm^{-1}$ | correlation coefficient |
|---|---|---|---|---|---|---|---|
| 310* | 0.175 | 0.900 | 2.8 | 4.07 | 1.97 | 3.0 | 0.872 |
| 330* | 0.270 | 1.041 | 2.6 | 1.591 | 1.95 | 2.8 | 0.878 |
| 350* | 0.390 | 3.671 | 2.0 | 0.746 | 1.90 | 2.7 | 0.878 |
| 310** | 4.000 | 0.900 | 9.2 | 4.07 | 0.45 | 1.7 | 0.993 |
| 330** | 6.500 | 1.041 | 7.5 | 1.591 | 0.44 | 1.5 | 0.962 |
| 350** | 8.800 | 3.671 | 6.0 | 0.746 | 0.43 | 1.4 | 0.897 |

*Set a (m=1, n=1).
**Set b (m=3, n=1).

Figure 1. Experimental setup for the fixed bed catalytic tests: 1) $N_2$ gas supply 2) mass flow controller 3) evaporator 4) heater shell 5) reactor's bed 6) temperature controller 7) methanol supply 8) Dosing pump 9) condenser 10) separator 11) off gas line to GC 12) off liquid line.
Figure 2-a. FTIR spectrum of raw clinoptilolite zeolite used in this study.
Figure 2-b. FTIR spectrum of the modified clinoptilolite zeolite (catalyst) used in this study.
Figure 3. TPD diagram of the catalyst used in this study.
Figure 4. Effectiveness factor as a function of particle average size.
Figure 5. Average reaction rate as a function of MeOH average partial pressure throughout the differential reactor.
Figure 6.-a. Simulated (markers) and experimental (set a: m=1, n=1, dashed lines) data for the average reaction rate as a function of average methanol partial pressure in the absence of initial water.
Figure 6.-b. Simulated (markers) and experimental (set b: m=3, n=1, dashed lines) data for the average reaction rate as a function of average methanol partial pressure in the absence of initial water.
Figure 7.-a. Simulated (markers) and experimental (set a: m=1, n=1, dashed lines) data for the average reaction rate as a function of average methanol partial pressure in the absence of initial water.
Figure 7.-b. Simulated (markers) and experimental (set b: m=3, n=1, dashed lines) data for the average reaction rate as a function of average methanol partial pressure in the presence of initial water.



Figure 1. Experimental setup for the fixed bed catalytic tests: 1) $N_2$ gas supply 2) mass flow controller 3) evaporator 4) heater shell 5) reactor's bed 6) temperature controller 7) methanol supply 8) Dosing pump 9) condenser 10) separator 11) off gas line to GC 12) off liquid line.

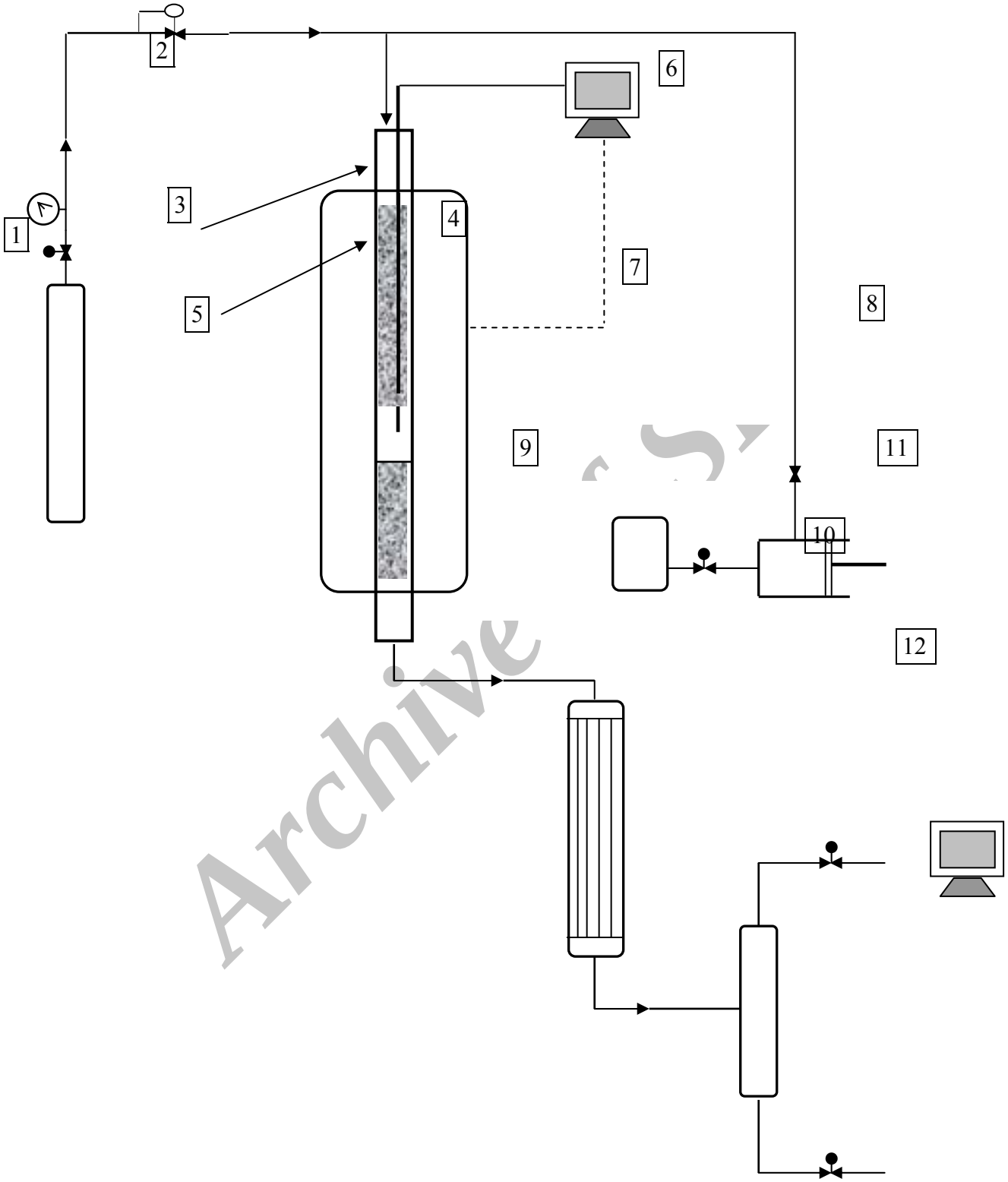

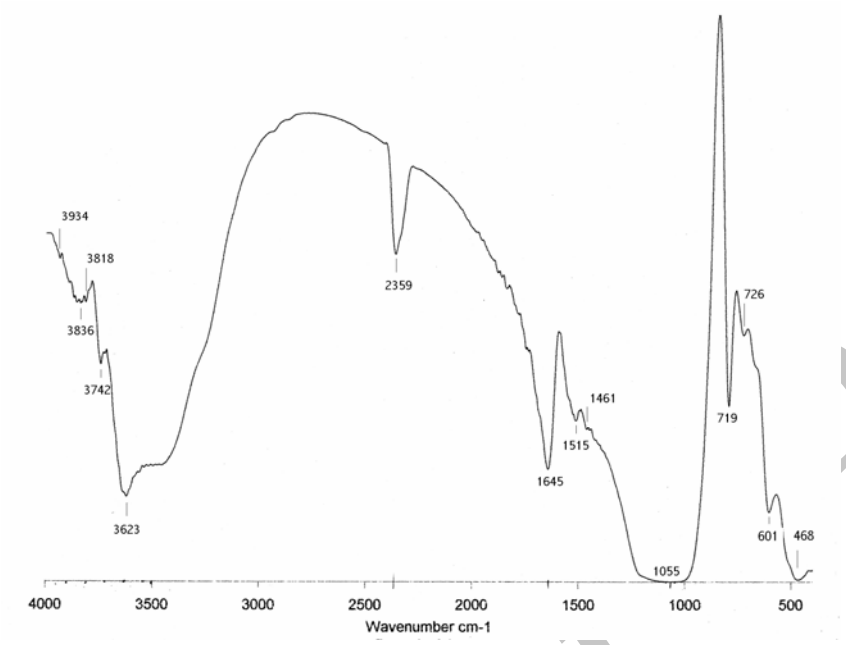


Figure 2-a. FTIR spectrum of raw clinoptilolite zeolite used in this study.

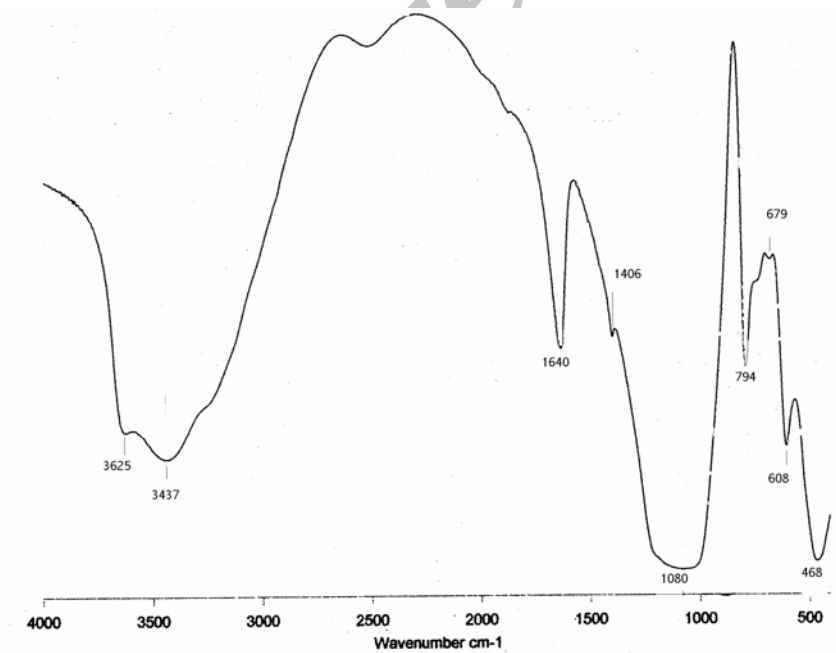


Figure 2-b. FTIR spectrum of the modified clinoptilolite zeolite (catalyst) used in this study.

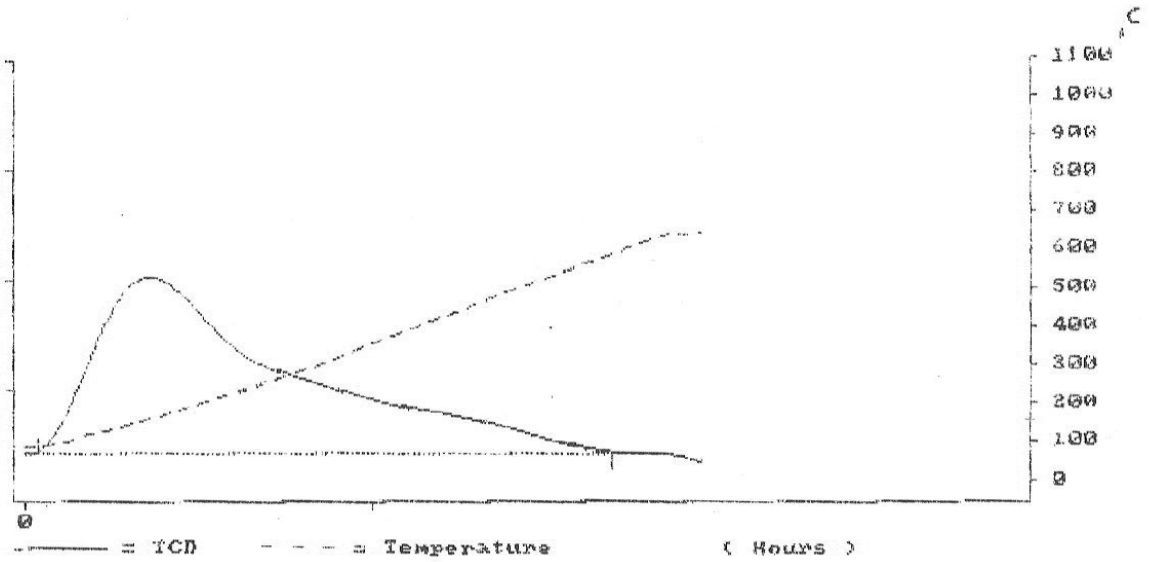


Figure 3. TPD diagram of the catalyst used in this study.

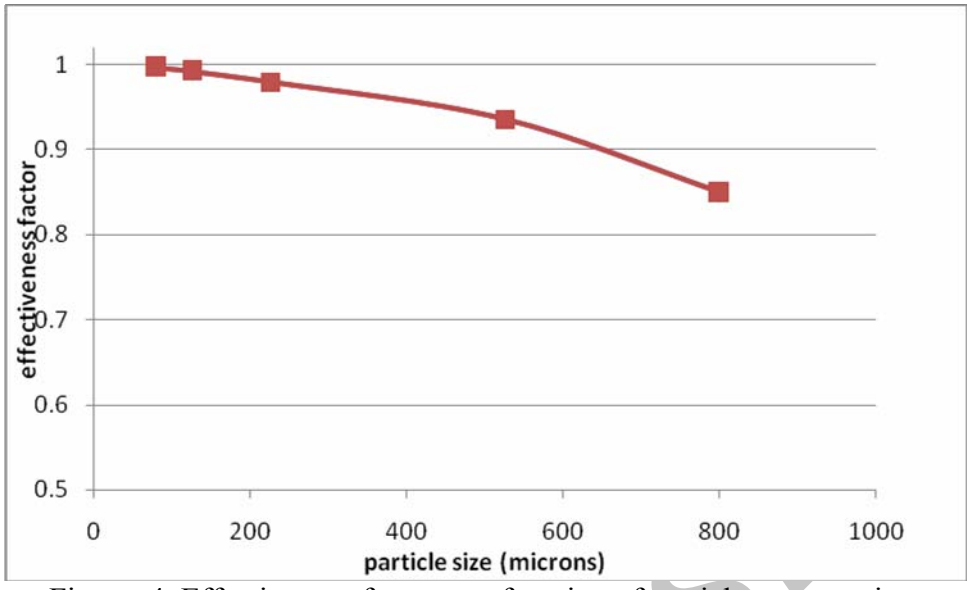


Figure 4. Effectiveness factor as a function of particle average size.

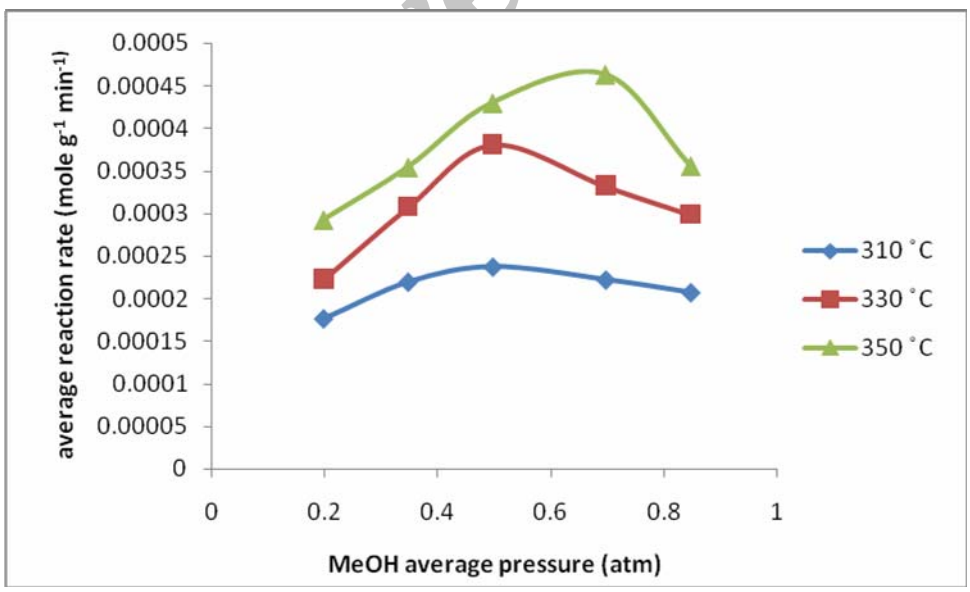


Figure 5. Average reaction rate as a function of MeOH average partial pressure throughout the differential reactor.

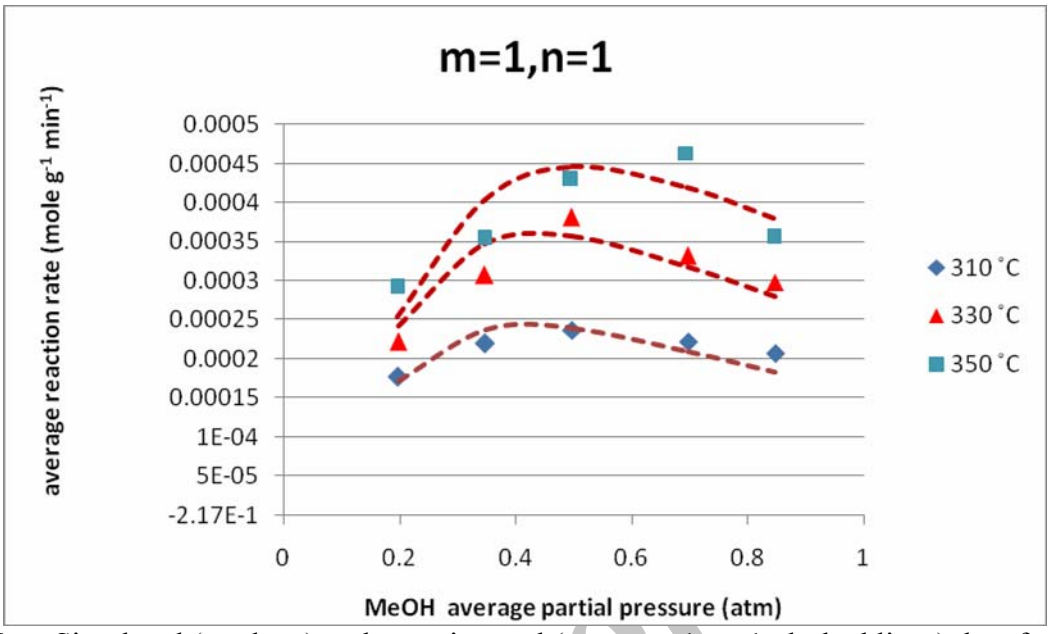


Figure 6.-a. Simulated (markers) and experimental (set a: m=1, n=1, dashed lines) data for the average reaction rate as a function of methanol average partial pressure in the absence of initial water.

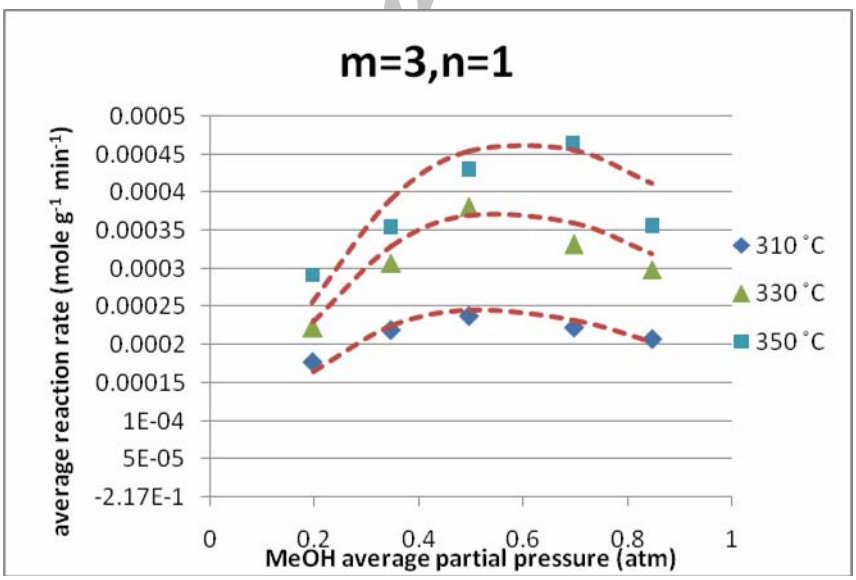


Figure 6.-b. Simulated (markers) and experimental (set b: m=3, n=1, dashed lines) data for the average reaction rate as a function of methanol average partial pressure in the absence of initial water.

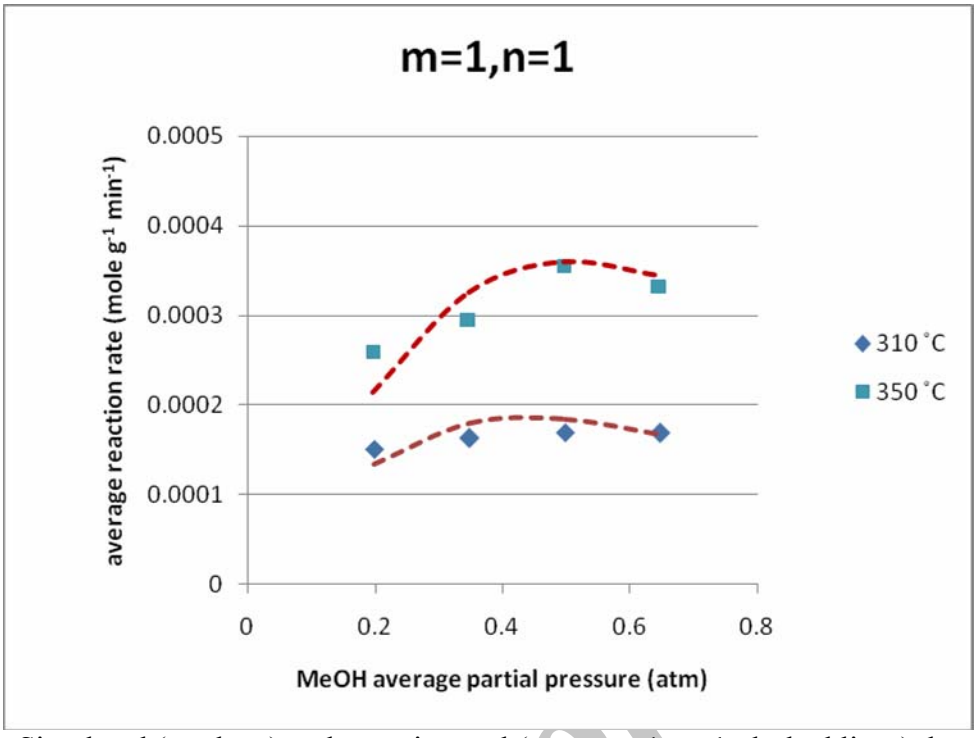


Figure 7.-a. Simulated (markers) and experimental (set a: m=1, n=1, dashed lines) data for the average reaction rate as a function of methanol average partial pressure in the absence of initial water.

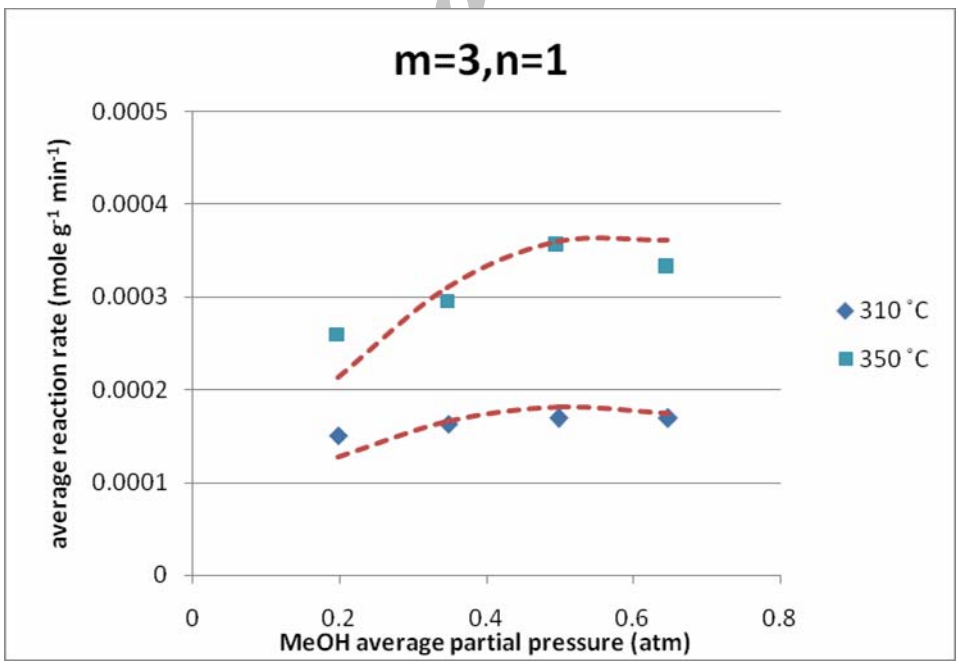


Figure 7.-b. Simulated (markers) and experimental (set b: m=3, n=1, dashed lines) data for the average reaction rate as a function of methanol partial pressure in the presence of initial water.